Available online at www.sciencedirect.com
SCIENCE DIRECT®
Journal of Power Sources 129 (2004) 7–13
JOURNAL OF POWER SOURCES
www.elsevier.com/locate/jpowsour

Contact thermal resistance of Li-ion cell electrode stack

Rengasamy Ponnappan [a,*], T.S. Ravigururajan [b]

[a] *Propulsion Directorate, Air Force Research Laboratory, Wright-Patterson AFB, Ohio, OH 45433-7251, USA*
[b] *Department of Mechanical Engineering, Wichita State University, Wichita, KS 67260-0133, USA*

Abstract

Lithium-ion batteries are widely used for portable energy storage in space power and consumer electronics applications. While the performance of these batteries is mainly depended upon the electrochemical aspects and contact electrical resistance of the cell stack, issues relating to *contact thermal resistance* between various layers of the cell stack could become more relevant under high rate of charge/discharge and extreme temperature operating conditions. An experimental program was carried out to establish the contact thermal resistance of a typical cell stack comprising graphite-coated copper anode, lithium cobalt oxide-coated aluminum cathode, polyethylene/polypropylene separator and electrolyte under various contact pressures and temperatures. The cell stack was not electrically charged or discharged during present experiments. Tests were conducted over a range of temperatures from −20 to 50 °C and pressures from 0 to 250 psi (1.72 MPa). The results show that, in general, resistance increases with decreasing pressure and the effect is significant when the pressure is reduced below 100 psi. Damage to the separator due to hot spots was observed at interface temperatures greater than 80 °C. Present results indicate that extreme operating temperatures may affect the performance of Li-ion batteries.

Keywords: Thermal resistance; Contact pressure; Li-ion cell electrode layers; Temperature and pressure measurement; Electrode stack packaging; Separator hot-spot; Battery thermal design data

1. Introduction

Aerospace and automotive applications require lightweight rechargeable batteries. Lithium-ion batteries are currently used as secondary power storage devices by the electronic and consumer industries. Compared to other rechargeable batteries, Li-ion batteries exhibit better characteristics in terms of capacity, power and energy density, charge retention and life cycles and these batteries were first used successfully in the Mars 2001 Lander mission [1]. The performance of these batteries is dominated by electrochemical aspects such as kinetics of lithium intercalation/de-intercalation, ionic mobility of species in the electrodes and electrolyte, interfacial properties and polarization effects and contact electrical resistance. Under normal operating conditions, contact thermal resistance may not be having a decisive impact on the cell performance; however, it may become more relevant under extreme operating conditions. A clear knowledge of the thermal and electrical contact resistances and their correlation, if any, of the electrode stack is useful in understanding cell behavior. The microstructure, crystalline nature, texture, and morphology of carbon and graphite materials are improved through various manufacturing processes [2]. Beginning with the first demonstration in 1980 [3], Li-ion batteries have advanced the battery technology substantially. The commercialization of Li-ion technology began in 1991 and the design continues to improve. The state-of-the art 18 650 size commercial cell typically delivers up to ∼1.8 A h for use in portable applications. A cutaway view of a typical prismatic Li-ion battery is shown in Fig. 1.

Contact pressure on the electrode stack during the operation of a battery will vary depending upon the initial assembly pressure and on the operating temperature. This variation will affect the internal heat transfer from the stack to the containment shell and in turn influence the external thermal design of the battery and its mounting environment in any electronics system. In order to calculate the heat dissipation into or out of the battery, a set of reliable experimental data for the parameter contact thermal resistance as a function of pressure and temperature is required by the thermal designer. As the Li-ion battery technology and the electrode stack materials are still evolving, these data are not available currently in the published literature. The contact thermal resistance of the electrodes and the separators is often assumed to be independent of

* Corresponding author.
E-mail address: rengasamy.ponnappan@wpafb.af.mil (R. Ponnappan).

0378-7753/$ – see front matter © 2003 Elsevier B.V. All rights reserved.
doi:10.1016/j.jpowsour.2003.11.006

Nomenclature

c_p	specific heat (J/kg K)
I	current (A)
R	thermal resistance (m^2 K/W)
T	temperature (°C)
V	voltage (V)
V	volume flow rate (m^3/h)
x	distance (mm)
k	thermal conductivity (W/m K)
r	density (kg/m^3)

Subscript

c,i	coolant inlet
c,o	coolant outlet
Cu	copper
5,e	interface edge of the heated section on the copper rod
6,e	interface edge of the cooled section on the copper rod

temperature and pressure or mostly approximate empirical values.

Various published thermal models that provide valuable insight into the thermal characteristics of a Li-ion cell, had to make several assumptions regarding the thermal conductivity/resistance characteristics. While analytical solutions by Carslaw and Jaeger [4] and Crank [5] give restricted solutions to highly simplified governing equations, most analyses are based on computational techniques. For example, Subramaniam and White [6], and Matlosz and Newman [7] used finite difference method (FDM) to analyze the thermal characteristics of a Li-ion cell. Never the less, the thermal models describing the Li-ion cells are based on idealized conditions. Chen and Evans [8,9] developed two- and three-dimensional models to study prismatic Li-ion batteries. Their model assumed uniform heat generation and required charge–discharge (I–V) curves to estimate the heat generation. Kanari et al. [10] employed an energy balance approach to the techniques followed by Chen and Evans [9]. Roth [11] and Pals and Newman [12] developed a one-dimensional thermal model for a single cell and multi-cell stack [12] assuming a constant temperature throughout the cell stacks. However, one major assumption in these studies is that the transport properties are independent of temperature. The need for a temperature-dependent property evaluation is well recognized by Botte et al. [13], who derived the complete energy balance and cited the lack of accurate estimation of controlling parameters.

The present experimental study seeks to fill some of the gap by investigating the contact thermal resistance of the most commonly used electrodes in a Li-ion cell, as a function of temperature and pressure. This paper describes an experimental study to determine the thermal contact resistance of electrodes with and without an electrolyte at various contact pressures and temperatures. The simulated cell stack with electrolyte was not charged with electrical potential during the tests for simplicity. Also, no measurement was done to monitor the electrical resistance of the stack. An experimental research involving the above complexities is beyond the scope of the present effort but however promising to be addressed in future research.

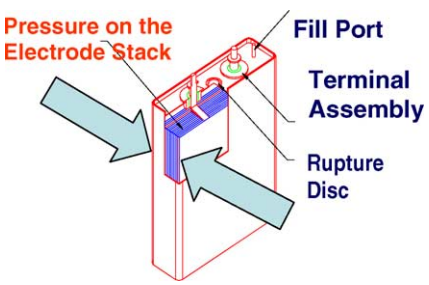

Fig. 1. A typical Li-ion battery.

2. Description of experiment

2.1. Test set-up

A table-top experimental set-up as shown in Fig. 2 was designed and built. The set-up consists of a vertically oriented copper-rod test-section which is divided into two halves, one heating section with a heat input through a dc power source and the other a cooling section cooled through a circulating constant temperature bath that can be maintained at any desired temperature between −25 and 50 °C. A secondary gear pump driven by a variable speed motor circulates the coolant to the cooling section and back to the cool bath. A piston type flow meter measures the small volumes of the ethylene glycol–water mixture that flows through the test

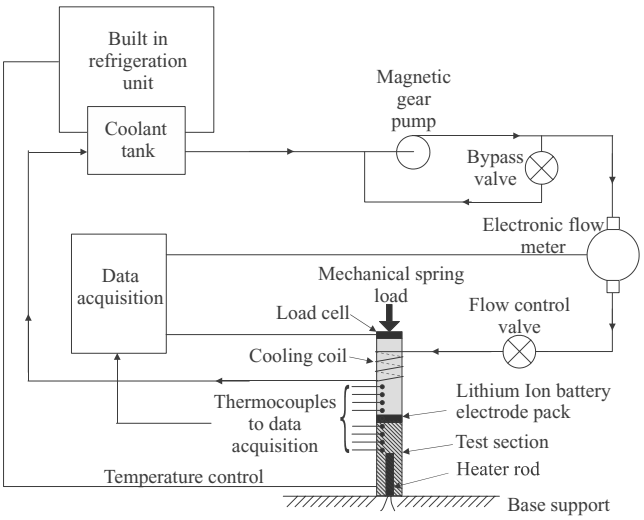

Fig. 2. A schematic diagram of the experimental set-up.

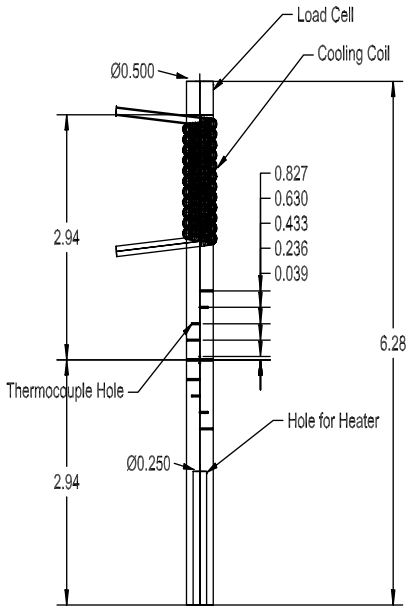

Fig. 3. Details of the test section (dimension in inches).

section. The electric power to the test section is supplied by a regulated dc power supply. The bath temperature, the flow rate, and power input to the test section are controlled by the data acquisition system program run on a PC.

2.2. Test section

The test section is made of two identical solid copper cylindrical rods kept in mechanical contact with each other along the axial direction (Fig. 3). This contact houses the electrode stack samples. The bottom part is heated using a cartridge heater placed inside along its axis. The top part contains the calorimetric section made up of a 1/16 in. copper tube wound and soldered around the circular solid copper rod. The copper tubing is connected by appropriate fittings to the secondary loop of the main set-up. Five thermocouples are placed on each of the copper rods along the length on either sides close to the contact interface between the heated and cooled test sections as shown in Fig. 3. These thermocouples are offset from each other circumferentially at different angles and depths. The two contacting faces of the copper rods are ground and polished to make a good contact. A frame holds the copper test section upright. Mechanical load on the test section is applied using a calibrated spring loaded plate placed at the top of the calorimetric section. A load cell is used to measure the axial load. The test section is insulated at both ends with phenol-resin insulators and wrapped with two layers of insulating blankets. The piping and the constant temp bath are also insulated to minimize the heat gain to the coolant. The test section thermocouples, the control thermocouple from the cold-bath and the flow controls signals are connected to the HP-3825 data acquisition system which is in turn interfaced with the PC. The data acquisition program controls the various inputs to the test loop. The program also monitors and gathers data on demand by the user.

2.3. Test specimen

The test specimens were research samples of electrode materials obtained from a Li-ion battery manufacturer and these samples do not represent any particular standard Li-ion battery electrode stack. Physical details of the present samples are as follows:

Size of specimen: circular disc 0.5 in. diameter.
Anode: graphite with binder (LiC_6) on copper; Cu film thickness = 0.001 in.; total thickness with dark gray coating on both sides = 0.0061 in.
Cathode: lithium cobalt oxide ($LiCoO_2$) with binder and carbon as conductor on aluminum; Al film thickness = 0.0011 in.; total thickness with dark gray coating on both sides = 0.0079 in.
Separator: polyethylene/polypropylene (PEPP) film; thickness = 0.001 in.; porosity = 40–45%.
Electrolyte: lithium hexafluoride phosphate ($LiPF_6$) salt solution in a mixture of diethyl/ethylene carbonates (not to be exposed to water or oxygen).

2.4. Test procedure

The computer and the data acquisition system units are first started and the program loaded into the computer memory. Using the program the bath temperature is set to the desired value. The secondary pump is run at a nominal flow rate of about 1–2 cc/min. Once the bath temperature is stabilized, the test section is allowed to reach a steady state and the data gathered for zero-power input to serve as the reference. At this point all thermocouples read the same temperatures within $\pm 0.5\,^{\circ}C$. This system check is usually done by setting the bath temperature near to the ambient temperature. Following the reference setting, power is input to the heater at desired levels. The test section is allowed to reach a steady state, after which the data is logged. Pressure is varied by tightening or loosening the spring loaded bolts, and the flow rate could be adjusted, if necessary, in order to facilitate the system to reach a steady state. Data are taken at various power levels for each axial load level setting and this was repeated for all desired loads. The experiment is repeated for five different contact specimen configurations.

(1) plain copper rods in contact: Cu–Cu;
(2) graphite coated copper anode film sandwiched between copper rods: Cu–anode–Cu;
(3) lithium cobalt oxide coated aluminum cathode film between copper rods: Cu–cathode–Cu;
(4) PEPP separator film between copper rods: Cu–separator–Cu;
(5) anode, cathode and separator stack with and without electrolyte pack between copper rods: Cu–anode–separator dry/wet-cathode–Cu.

The simulated electrode stack specimens are not expected to cause any adverse thermal or electrochemical effects with the copper pressure contacts as far as the heat flow through the interface is concerned.

The thin-film battery-electrode specimens are placed between the test sections and the experiments are carried out under dry conditions. After these series of dry tests, all the experiments are repeated with the specimens saturated with the electrolyte and placed between the two sections of the copper rods. The interface is immediately sealed carefully with a room temperature vulcanizer (silicone-based RTV). The test section is allowed to set for 2 h and then the experiments are conducted. After the experiments, the test sections are opened out to make sure that the test specimens still retained the electrolyte. All the data are logged into separate files in ASCII format for easy data reduction in any standard software.

2.5. Data reduction

The temperature, flow, and power input measurements are used to calculate the contact resistance of the specimen. The energy balance is obtained by matching the power input to the heat gained by the glycol mixture at the sink, which is given as follows:

$$\mathrm{V}rc_{\mathrm{p}}(T_{\mathrm{c,o}} - T_{\mathrm{c,I}}) = VI \tag{1}$$

The energy balance was consistently more than 90% when the bath temperature was above 10 °C. Also, the energy flow can be verified by the temperature profile along the rod, which is consistently linear for all temperatures of the bath and the all specimens. The closest thermocouples are 1 mm from the copper interface. The interface temperature is therefore estimated by linearly extrapolating the measured temperature profiles of both sections. With these two edge temperatures at the interface known, the interface resistance is found accurately by matching the energy balance across the interface with the heat flow between the two preceding thermocouple locations:

$$-k_{\mathrm{Cu}}\frac{(T_5 - T_4)}{(x_5 - x_4)} = \frac{(T_{5,\mathrm{e}} - T_{6,\mathrm{e}})}{R} \tag{2}$$

The contact resistance R for the specimen, based on unit area of cross-section, is given as:

$$R = \frac{(T_{5,\mathrm{e}} - T_{6,\mathrm{e}}) \times (x_5 - x_4)}{(T_5 - T_4) \times k_{\mathrm{Cu}}} \tag{3}$$

In this data reduction, temperature effects on copper thermal conductivity and the glycol properties are taken into account [14].

3. Results and discussion

The test results are presented in two groups, one where the specimens are either anode/cathode/separator films without the electrolyte (*dry tests*); and the other where the separator or the total electrode stack is soaked with the electrolyte (*tests with electrolyte*). Temperature profiles along the length of the test section and contact thermal resistance values as a function of contact pressure and temperature are presented for various specimens.

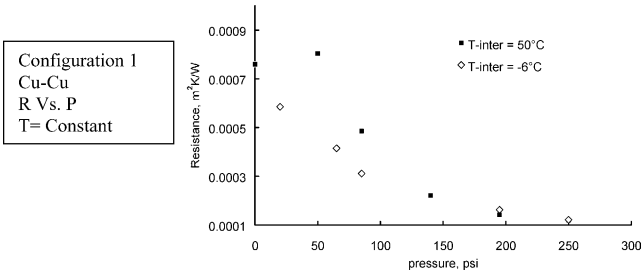

Fig. 4. Contact resistance variation with contact pressure at low and high interface temperatures.

3.1. Dry tests

The reduced data are presented for the case of interface between the two copper sections—Configuration 1 (Figs. 4 and 5). The pressure effect on the contact resistance decreases with increasing pressure. The contact resistance is significantly higher at lower pressure, that too when the interface temperature is at around 50 °C. The difference between the resistance values becomes small for pressures greater than 125 psi (862 kPa). It is inferred that the grain structures of both polished interfaces do not mesh properly at low pressures; and at higher pressures the applied pressure in conjunction with thermal expansion is causing the improved contact. The experiments were repeated several times and this trend continued, as expected (Fig. 4). The contact resistance did not change noticeably with the testing range and the value generally agreed with the published thermal contact resistance values for copper [15]. Also, the temperature profiles shown in Fig. 5 indicate the validity of the temperature measurements. Here, one can see the expected linear temperature profiles along the length of the test section as also their behavior with pressure variations in accordance with expected trends. When a specimen is inserted at the interface, each copper surface makes perfect contact with either side of the specimen. Graphs of temperature profiles

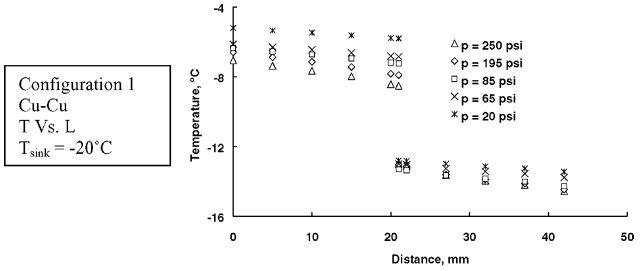

Fig. 5. Copper–copper test section temperature profiles at −20 °C sink temperature and at different contact pressures.

for all the above discussed cases show remarkably agreeable trends. The profiles are linear along both the heating as well as the cooling sections. The pressure effect is as anticipated but it had a more pronounced impact on the temperature profiles at the heating section than at the cooling section.

Temperature effects on the contact resistance of the anode/cathode are shown in Fig. 6. The effect of pressure on the anode specimen follows closely the trends exhibited by the copper surfaces. The difference in resistance due to environment temperature is negligible for $p = 250$ psi. Also the resistance is lower than that of the contact resistance of the copper interfaces. This is to be expected because the anode is made of copper coated with graphite and makes a much better contact with copper interfaces. One should note that the anode resistance is that of the anode composite material itself and the data shown for copper is that of the contact resistance and not that of the copper material itself. The anode resistance is independent of temperature variation at the interface. There is a slight decrease in resistance when the sink temperature is lowered to $-2\,^{\circ}$C (Fig. 6).

The resistance of cathode composite specimen is much higher than that of the plain copper interface, and even higher than that of the anode. The trends are similar to that of the anode. The data for the sink temperature of $-10\,^{\circ}$C is actually within the range and they are plotted against the average interface temperature. The pressure effects (not shown) on anode/cathode are also similar to that of the anode data with negligible environment effect for $p = 250$ psi. It was observed from the experiment that the resistance increases dramatically as the pressure is reduced below 125 psi and the sink (environment) temperature plays an increasingly important role in raising the resistance.

Figs. 7 and 8 show the test results on PEPP insulating separator. While the higher resistance of the separator is fully recognized, it differs from the electrodes in that the environment temperature continues to affect the resistance irrespective of the pressure. Actual resistance of the insulator is markedly higher by almost 600%.

Fig. 9 shows the results for tests on the dry stack consisting of an anode and cathode separated by the separator film. As can be seen from the figures, the resistance is dominated by the separator and the trends and the overall values are closer to that of the insulating separator. The difference in resistance due to the sink temperature is significantly less. The slight increase in resistance due to increase in temperature on the dry stack is not clear. The experimental set-up may have to be modified to obtain more detailed data over a wider temperature range. However, it appears that the stack resistance is dictated by that of the separator. The decreasing trend in resistance at the low interface and sink temperatures resembles that of the electrodes and that of the separator.

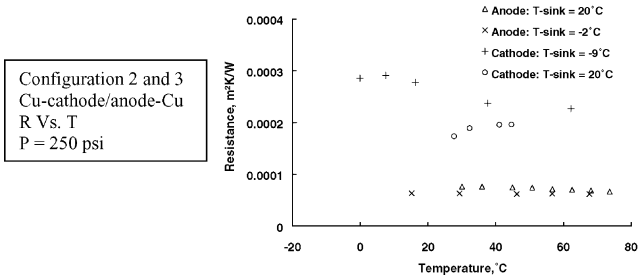

Fig. 6. Contact resistance variation with interface temperature at various sink temperatures and $p = 250$ psi; Configurations 2 and 3.

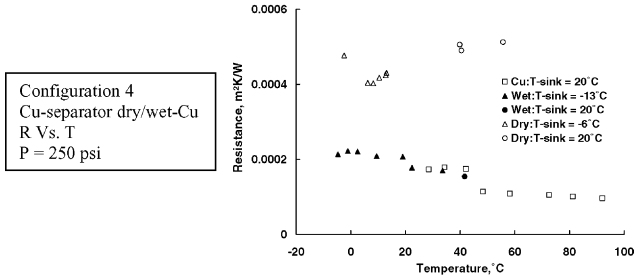

Fig. 7. Contact resistance variation with interface temperature at various sink temperatures and $p = 250$ psi; Configuration 4.

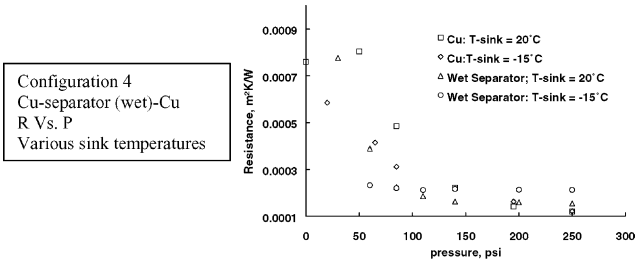

Fig. 8. Resistance vs. interface pressure; Configuration 4 with PVDF separator with electrolyte.

3.2. Tests with electrolyte

In Li-ion batteries, the electrolyte is stored to a large extent in the pores of the separator and to a lesser extent in the anode and the cathode coatings. The test results on the separator and the stack are shown in plots (Figs. 10 and 11). The pressure effects shown in Fig. 10 indicate very little influence due to the sink temperature. The temperature profiles of the separator and the stack in the presence of electrolyte is predictably similar to those of other profile plots, but the profiles are closely packed with the little effect of pressure.

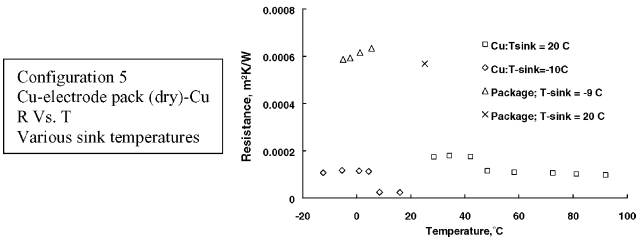

Fig. 9. Resistance vs. interface temperature; Configuration 5 with dry electrode pack.

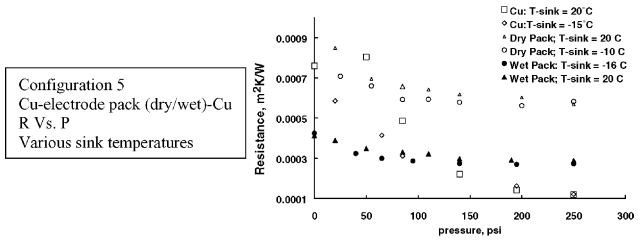

Fig. 10. Effect of interface pressure on resistance of electrode assembly without and with electrolyte.

The resistance is reduced considerably in the presence of the electrolyte. It is now in-line with that of the plain copper interface. Another interesting aspect is the absence of sink temperature effect on the resistance. The pressure effects are noticeable only when the sink temperature is at 20 °C. At the lower sink temperature of −15 °C the resistance is almost independent of pressure. The apparent pressure effect may be attributed to partial drying or depletion of the electrolyte from the separator at higher pressures. It is interesting to note that the general trend follows that of the dry plastic separator. Results from tests on the stack wetted with the electrolyte are interesting in that over a given temperature range the resistance is higher for the lower temperature of the bath. Also, when the bath (or sink) temperature is increased, the resistance equalizes for interface temperatures above 60 °C (Fig. 11).

During the course of the experiments, it was noticed that the separator started thinning out locally, perhaps due to hot spots. This has an adverse effect on the whole stack, because the stack resistance is dominated by that of the separator. Also, as the temperature increased and the pressure is applied, the coating on the anode started to peel off. The presence of electrolyte remarkably reduces the resistance. It should be noted that the test section was sealed after the introduction of the electrolyte. At the conclusion of each test, the electrodes were checked for the presence/absence of electrolyte. Data from several tests runs were discarded since it was suspected that imperfect sealing left the electrodes somewhat dry. Also discarded were the data for runs, wherein, a hole was noticed in the separator. Only test runs which did not result in a “through hole” were included. The authors noticed that the electrodes were damaged around 90 °C. The tests were therefore conducted such that the stack

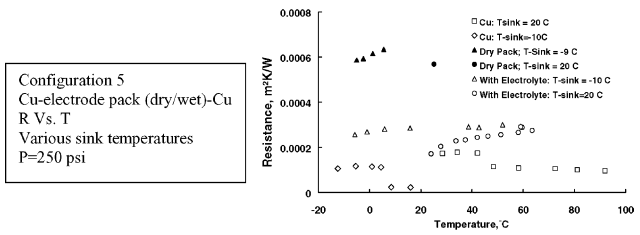

Fig. 11. Effect of interface temperature on resistance of electrode assembly without and with electrolyte.

temperatures were less than 80 °C. At these temperatures, on completion of the tests, “thinning” of the separators were noticed.

Also, the impact of the contact thermal resistance on charging/discharging and the State of Charge (SoC) of a Li-ion battery is not well established. However, it is intuitive to assume that the charge/discharge cycling and the internal heat generation would result in expansion/contraction of the electrode stack which consequently would increase/decrease the contact pressure within the stack. And that is the primary reason for this experimental measurement. At least one study has indicated that the chemical reactions that occur at the electrodes during charging/discharging process can lead to “thermal runaway” in cells when the cells are fully charged [11]. Based on that implication, we can expect the repeated charging/discharging of Li-ion batteries would lead to variations in contact thermal resistance within the stack. Further studies would likely provide new knowledge of how to package the electrode stack and what optimum preloading should be allowed during assembly in order to assure extended life for the cells.

4. Conclusions

The following conclusions were drawn from this study:

1. Experimental set-up was verified for standard Cu–Cu contact resistance data for pressure and temperature ranges of interest.
2. The literature data range found for various Cu–Cu contacts is $R_c = 0.00002–0.002\ m^2\ K/W$. Cu–Cu contact resistance does not vary with temperature but decreases considerably with increase in pressure—an anticipated trend.
3. Wet electrode stack has lower resistance (2–2.5 times) compared to dry stack.
4. Temperature variation has only slight effect on the stack resistance (wet or dry).
5. Pressure variation does not affect the wet stack resistance as much as that of the dry stack. This indicates that the electrolyte provides a good thermal contact for the electrodes. Dry stack resistance decreases with increase in pressure.
6. For a given pressure, the electrode stack has higher resistance (dry stack is six times higher; Wet stack is two to three times higher) compared to Cu–Cu contact resistance because of the polymer separator layer.
7. Damage to the polymer separator layer is very likely if unexpected hot spot development occurs at temperatures >50 °C. This could affect battery performance adversely.
8. These experimental thermal contact resistance data could be useful for battery thermal dissipation, packaging and life prediction calculations.

Acknowledgements

This study was funded in part by the AFOSR through an NRC summer fellowship to the university author and performed at the Thermal Laboratory, Energy Storage and Thermal Sciences Branch. The authors thank Dick Marsh, Brian Hager, Steve Vukson and John Erbacher (AFRL/PRPS) for their inputs and support of this research and Richard Harris (UDRI) for his help building the experimental set-up.

References

[1] M.C. Smart, B.V. Ratnakumar, L. Whitcanack, S. Surampudi, J. Byers, R. Marsh, IEEE Aerospace Elect. Syst. Mag. 14 (1999) 36.
[2] A. Saiko, T. Muramatsu, H. Arai, NEC R&D, vol. 41, No. 1, NEC Creative Ltd., 2000, p. 28.
[3] M. Lazzari, B. Scrosati, J. Electrochem. Soc. 1, 2, 7 (1980) 773.
[4] H.S. Carslaw, J.C. Jaeger, Conduction of Heat in Solids, Oxford University Press, London, 1993, p. 242.
[5] J. Crank, Mathematics of Diffusion, Oxford University Press, London, 1994.
[6] V.R. Subramaniam, B.S. Haran, R.E. White, Comput. Chem. Eng. 23 (1999) 287.
[7] M. Matlosz, J. Newman, Comput. Chem. Eng. 11 (1987) 45.
[8] T. Chen, J.W. Evans, J. Electrochem. Soc. 140 (1993) 1833.
[9] T. Chen, J.W. Evans, Electrochem. Acta 39 (1994) 517.
[10] K. Kanari, K. Takano, Y. Saito, T. Masuda, in: Proceedings of the International Workshop on Advanced Batteries, Osaka, 1995.
[11] E. Peter Roth, in: Proceedings of the 39th Power Source Conference, June 2000, pp. 128–131.
[12] C.R. Pals, J. Newman, J. Electrochem. Soc. 142 (1995) 3282.
[13] G.G. Botte, B.A. Johnson, R.E. White, J. Electrochem. Soc. (1999) 1370.
[14] R.H. Perry, Chemical Engineers Handbook, 7th ed., McGraw-Hill, New York, 1997.
[15] F.P. Incropera, X.Y. DeWitt, 1999, Fundamentals of Heat and Mass Transfer, 5th ed., McGraw-Hill, New York, 1999.